Inverse Problems **25** (2009) 025004 (24pp) doi:10.1088/0266-5611/25/2/025004

An implicit radial basis function based reconstruction approach to electromagnetic shape tomography

Naren Naik[1], **Rick Beatson**[2], **Jerry Eriksson**[3] **and Elijah van Houten**[1]

[1] Department of Mechanical Engineering, University of Canterbury, Private Bag 4800, Christchurch-8140, New Zealand
[2] Department of Mathematics and Statistics, University of Canterbury, Private Bag 4800, Christchurch-8140, New Zealand
[3] Department of Computing Science, Umeå University, S-901, 87 Umeå, Sweden

E-mail: naren.naik@canterbury.ac.nz, rick.beatson@canterbury.ac.nz, jerry@cs.umu.se and elijah.vanhouten@canterbury.ac.nz

Received 9 May 2008, in final form 20 November 2008
Published 18 December 2008
Online at stacks.iop.org/IP/25/025004

Abstract
In a reconstruction problem for subsurface tomography (modeled by the Helmholtz equation), we formulate a novel reconstruction scheme for shape and electromagnetic parameters from scattered field data, based upon an implicit Hermite interpolation based radial basis function (RBF) representation of the boundary curve. An object's boundary is defined implicitly as the zero level set of an RBF fitted to boundary parameters comprising the locations of few points on the curve (the RBF centers) and the normal vectors at those points. The electromagnetic parameter reconstructed is the normalized (w.r.t. the squared ambient wave number) difference of the squared wave numbers between the object and the ambient half-space. The objective functional w.r.t. boundary and electromagnetic parameters is set up and required Frechet derivatives are calculated. Reconstructions using a damped Tikhonov regularized Gauss–Newton scheme for this almost rank-deficient problem are presented for 2D test cases of subsurface landmine-like dielectric single and double-phantom objects under noisy data conditions. The double phantom example demonstrates the capability of our present scheme to separate out the two objects starting from an initial single-object estimate. The present implicit-representation scheme thus enjoys the advantages (and conceptually overcomes the respective disadvantages) of current implicit and explicit representation approaches by allowing for topological changes of the boundary curve, while having few unknowns respectively. In addition, the Hermite interpolation based RBF representation is a powerful method to represent shapes in three dimensions, thus conceptually paving the way for the algorithm to be used in 3D.

(Some figures in this article are in colour only in the electronic version)

1. Introduction

Limited data reconstruction problems in electromagnetic tomography occur in a variety of application areas such as humanitarian demining, geophysical prospecting and medical imaging. In such problems, it is often meaningful to solve an 'approximate' reconstruction problem wherein the object shape, location and an approximate (as against pointwise) estimate of the object's electromagnetic parameters are evaluated [1–8]. The reconstruction of the desired parameters is typically achieved via a minimization of an objective functional comprising the residual of the measured and modeled data. The iterative 'shape based' approximate reconstruction schemes broadly fall into two categories. The objective functional minimized in the first class has as unknowns the coefficients in an explicit parametric representation for the boundary curve(s), while in the latter class, the unknowns are the values of a set function representing the image, with the zero level set of that function implicitly representing the boundary. While the first (explicit representation) class of schemes (as in [1, 4–8]) has the advantage of fewer unknowns, which is useful in potential three-dimensional reconstructions, the second (implicit representation) class (as in [2, 3]) is better suited to handle topological changes in the evolving shape of the boundary. A detailed literature survey of these various classes of schemes is given in [4, 7, 8]. In [9], a pointwise interpolated radial basis function (RBF) based level-set approach is proposed for shape and topology optimization, which assumes that the RBF centers are fixed through the time evolution of the initial curve.

The contemporarily developed works in optical [4] and subsurface tomography [8] on simultaneous electromagnetic and shape parameter reconstructions form a bridge between the two classes of schemes by using a level-set representation for the shapes in order to calculate shape and electromagnetic parameter Frechet derivatives of the objective functional in a parameterized explicit representation (spherical harmonics in [4] and B-splines in [8]) and not in the more customary implicit level-set representation of the boundaries. The shape Frechet derivatives in these works calculate the variation in the measured data w.r.t. infinitesimal variations in the level-set function representing the boundary, which in turn is calculated in terms of corresponding variations in the coefficients of the parametric expansion for the boundary. Their expressions are related to the boundary-integral expression of the seminal work of [10] giving variations of internal parameters w.r.t. infinitesimal boundary variations.

Radial basis functions are very useful general purpose approximators [11, 12], particularly when the data points are scattered rather than gridded. The radial basis function circle of ideas is usually presented in the context of interpolation to point values. It is less well known that the RBF ansatz extends to much more general observation functionals including Hermite data [13–15]. Computational experience (unpublished) with Hermite interpolatory RBFs suggests that they are superior to ordinary point value RBFs for implicit shape modeling, achieving the same quality of fit with significantly fewer parameters. In this paper, we utilize RBF Hermite interpolation to a mix of point values and directional derivatives to provide an *implicit* boundary-representation scheme that has few parameters; thus combining the advantages of previous implicit and explicit representation schemes. This yields a scheme that uses a shape representation with few unknowns, and that also can change the topology of the reconstructed curve away from that of the initial estimate. In particular, with the implicit RBF representation, we are fitting a minimal energy interpolant rather than specifying any particular topology *a priori*. The approximation is simply driven by the given data. We mention that our approach fundamentally differs from that of [9] in that we consider the motion of the centers as the iterations progress and use a Hermite RBF scheme as compared to their pointwise scheme.

In the present work, in the context of a subsurface reconstruction problem for GPR tomography (modeled by the Helmholtz equation), we formulate a novel reconstruction

scheme for shape and electromagnetic (e.m.) parameters from scattered field data, based upon an implicit Hermite interpolation based RBF representation of the boundary curve. An object's boundary is defined implicitly as the zero level set of an RBF fitted to boundary parameters comprising the locations of few points on the curve (namely the RBF centers) and the normal vectors at those points. The e.m. parameter reconstructed is the normalized (w.r.t. the squared ambient wave number) difference of the squared wave numbers between the object and the ambient half-space, and is represented by coefficients in a suitable global basis. The objective functional w.r.t. boundary and e.m. parameters is set up and required Frechet derivatives are calculated. Reconstructions are obtained by using an iteratively regularized Gauss–Newton scheme for this almost rank-deficient problem.

The present implicit-representation scheme thus extends the capability of the approaches in [4, 8] by allowing for topological changes, while retaining their advantage over conventional implicit representation schemes of having few unknowns. In addition, the Hermite interpolation based RBF representation is a powerful method to represent shapes in three dimensions, thus conceptually paving the way for the algorithm to be used in 3D.

The paper is organized as follows. Section 2 defines the basic shape-based tomography problem considered in our work. Section 3 considers the Hermite interpolation based RBF representation of the boundary curve, while the Frechet derivatives needed are evaluated in section 4. Section 5 presents the reconstruction algorithm and section 6 the numerical results, with the conclusions being the subject of section 7. Appendix A evaluates some Frechet-derivative related matrices and appendix B briefly presents the basic relations for method of moments based derivative calculations needed in the Frechet derivative calculations of section 4.

2. The shape-based subsurface tomography problem

The two-dimensional inverse scattering problem considered here is to recover the object's permittivity (denoted by $\epsilon(\mathbf{r}), \mathbf{r} \in \mathbb{R}^2$) and conductivity (denoted by $\sigma(\mathbf{r}, \omega), \mathbf{r} \in \mathbb{R}^2$) distributions from the measurements at various angular frequencies ω, of the scattered field obtained from the interaction of incident radiation with the object in question, on a receiver surface outside the object.

In the scalar approximation, the scattering process in GPR tomography is assumed to be modeled by the Helmholtz equation. The Helmholtz equation for the complex amplitude $u(\mathbf{r}, \omega)$ of a monochromatic wave of angular frequency ω, due to a source of current distribution $j(\mathbf{r}, \omega)$ propagating through a medium of complex wave number $k(\mathbf{r}, \omega)$, is given by

$$\Delta u(\mathbf{r}, \omega) + k^2(\mathbf{r}, \omega) u(\mathbf{r}, \omega) = j(\mathbf{r}, \omega), \tag{1}$$

where Δ is the Laplacian operator. The fields $u(\mathbf{r}, \omega)$ are assumed to be outgoing and satisfying the Sommerfeld radiation conditions at infinity. The complex wave number, $k(\mathbf{r}, \omega)$ is given by

$$k^2(\mathbf{r}, \omega) = \omega^2 \mu_0 \epsilon(\mathbf{r}) \left(1 + \mathrm{i} \frac{\sigma(\mathbf{r}, \omega)}{\omega \epsilon(\mathbf{r})}\right) \tag{2}$$

where μ_0 is the magnetic permeability of free space.

Define

$$f(\mathbf{r}) = \frac{k^2(\mathbf{r}, \omega) - k^2_{\mathrm{amb}}(\mathbf{r}, \omega)}{k^2_{\mathrm{amb}}(\mathbf{r}, \omega)}, \tag{3}$$

with $k(\mathbf{r}, \omega)$ being the wave number in the actual physical setting of the object(s) of interest embedded in an ambient medium corresponding to a wave number $k_{\mathrm{amb}}(\mathbf{r}, \omega)$. In the present

problem, the ambient medium comprises two half-spaces corresponding to air and ground, separated by an air–ground interface.

The independence of $f(\mathbf{r})$ on ω stems from the assumption that the quantity $\tan\delta \equiv \frac{\sigma(\mathbf{r},\omega)}{\omega\epsilon}$ does not vary with ω in the frequency range of interest [16].

The reconstruction problem is thus the recovery of $f(\mathbf{r})$ from the measurements at various angular frequencies ω, of the scattered field on the receiver surface.

Observing that the function $f(\mathbf{r})$ contains information about the parameter values as well as the shape, considering without loss of generality homogeneous inclusions in the background, we can express the parameter at a point in the image space, as

$$f(\mathbf{r}) = f^g(\mathbf{r})H[s(\mathbf{r})], \tag{4}$$

where $s(.)$ is a level-set based representation of the image ([10] and references therein) with $\{x : s(\mathbf{r}) = 0\}$ representing the boundary $\partial\Omega$ of the object(s) under consideration supported in region Ω, $H[.]$ is a Heaviside function taken in a suitable limiting sense [17] and the field quantity $f^g(.)$ can be considered as a 'ghost' parameter value manifesting itself through $H(.)$. Without loss of conceptual generality we set $f^g(\mathbf{r}) = \alpha$ in our work, with α being independent of position.

There are many ways in which one can represent the boundary curve/surface $s(\mathbf{r}) = 0$. In an explicit parametrization, this boundary has been described in terms of a spline basis ([1, 6, 8]) in two dimensions or with spherical harmonics [4] in three dimensions. In implicit formulations, typically the shape unknowns are the values of the function $s(\mathbf{r})$ on the reconstruction grid. On the other hand, in the present work, with the objective of retaining an implicit representation coupled with significant search-space-dimensionality reduction (as in explicit schemes), we represent $s(\mathbf{r})$ as a radial basis function via a Hermite interpolation scheme to fit a few on-curve points (called centers of the RBF, and denoted by $\mathbf{r}_1^c, \ldots, \mathbf{r}_m^c$) and the normal unit vectors at those points (denoted by $\mathbf{n}_1, \ldots, \mathbf{n}_m$ where $\mathbf{n}_i \equiv \left(\cos\theta_i^c, \sin\theta_i^c\right)$ for some θ_i^c). As explained in the following section, we can write the level-set function as an RBF of the form

$$s(\mathbf{r}) = p(\mathbf{r}) + \sum_{j=1}^{m}\left[c_j\Phi\left(\mathbf{r}-\mathbf{r}_j^c\right) - d_j\left(D_{n_j}\Phi\right)\left(\mathbf{r}-\mathbf{r}_j^c\right)\right], \tag{5}$$

where $p(.)$ is a polynomial (typically of low order), $\Phi(.) \equiv \phi(\|.\|)$, with ϕ being a (usually unbounded and non-compactly supported) real-valued function on $[0, \infty]$ called the basic function, and $D_{n_j}\psi(t) \equiv \mathbf{n}_j.(\nabla\psi)(t)$ denotes the directional derivative functional w.r.t. a unit normal $\mathbf{n}_j$.

Thus in the two-dimensional setting considered in our work, $\mathbf{r} \equiv (x, z)$, and, the shape parameters are the RBF-center coordinates $\left\{x_q^c \middle| q = 1, \ldots, M_p\right\}$, $\left\{z_q^c \middle| q = 1, \ldots, M_p\right\}$ along with the unit normals represented by the respective angles $\left\{\theta_q^c \middle| q = 1, \ldots, M_p\right\}$, corresponding in vector notation to $\mathbf{x^c}$, $\mathbf{z^c}$ and $\theta^{\mathbf{c}}$ respectively.

Setting

$$\mathbf{h} = \begin{pmatrix} \mathrm{Real}(\alpha) \\ \mathrm{Imag}(\alpha) \\ \mathbf{x^c} \\ \mathbf{z^c} \\ \theta^{\mathbf{c}} \end{pmatrix}, \tag{6}$$

the basic ill-posed reconstruction problem can be defined as solving for $\mathbf{h}$, the equation $\mathcal{A}(\mathbf{h}) = \mathbf{u_{data}}$. As is common practice, this problem is approximated by the following

Tikhonov regularized nonlinear c-minimum norm problem

$$\min_{\mathbf{h}} \tfrac{1}{2}(\|\zeta(\mathbf{h})\|^2 + \eta^2\|\mathbf{h} - \mathbf{c}\|^2), \tag{7}$$

where η is a regularization parameter, $\mathbf{c}$ is a known constant representing *a priori* information, which is typically taken to be the initial estimate of the iterative process (it can be changed within the iterative process to help stabilize the iterates), and,

$$\zeta(\mathbf{h}) = \begin{pmatrix} \mathrm{Real}(\mathbf{u_{data}} - \mathcal{A}(\mathbf{h})) \\ \mathrm{Imag}(\mathbf{u_{data}} - \mathcal{A}(\mathbf{h})) \end{pmatrix}, \tag{8}$$

where $\mathbf{u_{data}}\left(=\mathbf{u}^{\mathrm{rec}} - \mathbf{u}^{\mathrm{rec}}_{\mathrm{amb}}\right)$ is the 'effective' measured data vector, concatenated over the frequencies at which the measurements are taken, $\mathbf{u}^{\mathrm{rec}}$ is the measured field at the receiver and $\mathbf{u}^{\mathrm{rec}}_{\mathrm{amb}}$ is the ambient field that would have been measured at the receiver in the absence of the inhomogeneity. The functional $\mathcal{A} : \mathbb{R}^N \to \mathbb{C}^{M/2}$ is the measurement operator corresponding to the tomographic process, whose ith component (corresponding to the ith measurement) at the given frequency is $\mathcal{A}^i(\mathbf{h}; \omega, \mathbf{r}^i) \equiv u_{sc}(\mathbf{r}^i, \omega; f)$ (as defined in equation (B.3)), with $f(\mathbf{r}') = \alpha H[s(\mathbf{r}', \mathbf{h})]$, where N is the length of vector $\mathbf{h}$ and the number of measurements is $M/2$ (for later notational convenience). The measurement operator is obtained via a suitable discretization scheme (in the present work, a method of moments [18, 19] scheme is applied to the integral equation of scattering) to solve the Helmholtz equation for the scattered fields, given the object parameters.

In the present work, the minimization problem given by (7) is solved by using an iteratively regularized Gauss–Newton method that requires the computation of the Frechet derivatives of the received fields with respect to the parameter vector. These aspects along with the RBF representation scheme are dealt with in the following.

3. Hermite interpolation based RBF representation

Let $\gamma : \mathbb{R}^d \to \mathbb{R}$ be the level-set function, whose zero level set is the boundary curve to be reconstructed. Let $\mu_1, \ldots, \mu_m$ be point evaluation functionals

$$\mu_i(\gamma) = \delta_{\mathbf{r}^c_i}(\gamma) = \gamma\left(\mathbf{r}^c_i\right) \tag{9}$$

and $\mu_{m+1}, \ldots, \mu_{2m}$ be directional derivative evaluation functionals

$$\mu_{m+i}(\gamma) = \nu_i(\gamma) = (D_{\mathbf{n}_i}\gamma)\left(\mathbf{r}^c_i\right) = \mathbf{n}_i \cdot \nabla\gamma\left(\mathbf{r}^c_i\right). \tag{10}$$

These $2m$ functionals are linearly independent provided the points $\mathbf{r}^c_i$, $1 \leqslant i \leqslant m$, are distinct. Then our Hermite interpolation problem can be stated as

Problem 1. Given values $b_1, \ldots, b_{2m}$ find a continuously differentiable function $s : \mathbb{R}^d \to \mathbb{R}$ such that

$$\mu_i(s) = b_i, \qquad \text{for} \qquad i = 1, \ldots, 2m, \tag{11}$$

or equivalently such that

$$s\left(\mathbf{r}^c_i\right) = b_i \qquad \text{and} \qquad \mathbf{n}_i \cdot (\nabla s)\left(\mathbf{r}^c_i\right) = b_{m+i}, \qquad \text{for} \quad 1 \leqslant i \leqslant m. \tag{12}$$

Let π^d_{k-1} denote the space of polynomials of degree at most $k-1$ in d variables. Having chosen a twice continuously differentiable basic function Φ, conditionally positive definite of order k in the appropriate sense, we seek solutions to the RBF Hermite interpolation problem.

Problem 2. Find a function of the form

$$s(\mathbf{r}) = p(\mathbf{r}) + \sum_{j=1}^{m} \left[c_j \mu_j^{\mathbf{t}} \Phi(\mathbf{r}-\mathbf{t}) + d_j \nu_j^{\mathbf{t}} \Phi(\mathbf{r}-\mathbf{t})\right], \qquad p \in \pi_{k-1}^d, \tag{13}$$

$$= p(\mathbf{r}) + \sum_{j=1}^{m} \left[c_j \Phi\left(\mathbf{r}-\mathbf{r}_j^c\right) - d_j \mathbf{n}_j \cdot (\nabla\Phi)\left(\mathbf{r}-\mathbf{r}_j^c\right)\right], \tag{14}$$

satisfying the interpolation conditions (12) subject to the constraints

$$\sum_{j=1}^{m} c_j q\left(\mathbf{r}_j^c\right) + d_j \mathbf{n}_j \cdot (\nabla q)\left(\mathbf{r}_j^c\right) = 0, \qquad \text{for all} \quad q \in \pi_{k-1}^d. \tag{15}$$

The coefficients c and d are the RBF coefficients. An informative 1D analog is a C^1 piecewise cubic Hermite interpolant to data $\{t_i, f_i, f_i'\}$ which can be written as

$$s(t) = p(t) + \sum_{i=1}^{m} c_i |t-t_i|^3 - \sum_{i=1}^{m} 3d_i (t-t_i)|t-t_i|. \tag{16}$$

Constraint (15) takes away the extra degrees of freedom introduced by the polynomial p. It also lowers the rate of growth of the pure RBF part (in the square parentheses of (14)) as $|\mathbf{r}| \to \infty$. In the above the $\mathbf{t}$ superscript indicates that the functional is applied with respect to the $\mathbf{t}$ variable. Thus $\mu_j^{\mathbf{t}} \Phi(\mathbf{r}-\mathbf{t}) = \Phi\left(\mathbf{r}-\mathbf{r}_j^c\right)$ and $\nu_j^{\mathbf{t}} \Phi(\mathbf{r}-\mathbf{t}) = -\mathbf{n}_j \cdot (\nabla\Phi)\left(\mathbf{r}-\mathbf{r}_j^c\right)$. This is the so-called symmetric form of an RBF interpolation problem. Applying the interpolation conditions we obtain the RBF Hermite interpolation problem in the matrix form

$$\begin{bmatrix} A & P \\ P^T & O \end{bmatrix} \begin{bmatrix} \boldsymbol{\lambda} \\ \mathbf{a} \end{bmatrix} = \begin{bmatrix} \mathbf{b} \\ 0 \end{bmatrix}, \tag{17}$$

with the entries $A_{ij} = \mu_i^{\mathbf{r}} \mu_j^{\mathbf{t}} \Phi(\mathbf{r}-\mathbf{t})$, $P_{ij} = \mu_i(p_j)$, where $p(\mathbf{r}) = \sum_{l=1}^{L} a_l p_l(\mathbf{r})$ for some basis $\{p_1, \ldots, p_\ell\}$ for the space π_{k-1}^d and $\boldsymbol{\lambda} \equiv \binom{\mathbf{c}}{\mathbf{d}}$. The expressions for the entries in the matrices A and P of equation (17) are now given below. Firstly

$$P_{ij} = \mu_i(p_j) = \begin{cases} p_j\left(\mathbf{r}_i^c\right), & 1 \leqslant i \leqslant m, \\ \mathbf{n}_i \cdot \nabla p_j\left(\mathbf{r}_{i-m}^c\right), & m+1 \leqslant i \leqslant 2m. \end{cases} \tag{18}$$

Furthermore $A_{ij} = \mu_i^{\mathbf{r}} \mu_j^{\mathbf{t}} \Phi(\mathbf{r}-\mathbf{t})$ which implies

$$A_{ij} = \begin{cases} \Phi\left(\mathbf{r}-\mathbf{r}_j^c\right), & \text{if} \quad 1 \leqslant i, j \leqslant m, \\ -\mathbf{n}_{j-m} \cdot (\nabla\Phi)\left(\mathbf{r}_i^c - \mathbf{r}_{j-m}^c\right), & \text{if} \quad 1 \leqslant i \leqslant m, \text{ and } m+1 \leqslant j \leqslant 2m, \\ \mathbf{n}_{i-m} \cdot (\nabla\Phi)\left(\mathbf{r}_{i-m}^c - \mathbf{r}_j^c\right), & \text{if} \quad m+1 \leqslant i \leqslant 2m, \text{ and } 1 \leqslant j \leqslant m, \\ -\mathbf{n}_{i-m}^T H(\mathbf{r}_{i-m} - \mathbf{r}_{j-m}) \mathbf{n}_{j-m}, & \text{if} \quad m+1 \leqslant i, j \leqslant 2m, \end{cases} \tag{19}$$

where $H(\mathbf{r})$ is the $d \times d$ Hessian matrix with $h_{k\ell} = \frac{\partial^2}{\partial x_k \partial x_\ell}\Phi$. Thus we can write the matrix A in $m \times m$ block form as $A = \begin{pmatrix} A^{(11)} & A^{(12)} \\ A^{(21)} & A^{(22)} \end{pmatrix}$.

RBF Hermite interpolation is a multidimensional generalization of the well-known 1D Hermite piecewise cubic interpolation scheme. An early reference is [13], whose theory covers polyharmonic splines and pseudo splines, including the case of the basic function $\Phi(\mathbf{r}) = |\mathbf{r}|^4 \log(|\mathbf{r}|)$, supplemented with a quadratic polynomial considered here. Iske [14] gives a very general theory covering many choices of basic function. One piece of the general

theory useful to us is that if Φ is conditionally positive definite in the appropriate sense, the functionals $\{\mu_j\}$ are linearly independent over $C^1(\mathbb{R}^d)$, and also the functionals $\{\mu_j\}$ are unisolvent for π^d_{k-1} then the system (17), and the Hermite RBF interpolation problem (Problem 2), have a unique solution for any choice of right-hand side $\mathbf{b}$. Here unisolvent for π^d_{k-1} means that the only polynomial q so that $\mu_j(q) = 0$ for all $1 \leqslant j \leqslant 2m$ is the zero polynomial.

We are reconstructing a signed distance function, which is zero on the curve and has unit directional derivative in the direction of the inward normal. Thus, the right-hand side values we will use are $b_i = 0$ for $1 \leqslant i \leqslant m$, and $b_i = 1$ for $m+1 \leqslant i \leqslant 2m$. Hence, given the RBF centers $\{\mathbf{r}^c_j\}$, and the unit normal vectors at those points $\{\mathbf{n}_j = (\cos(\theta^c_j), \sin(\theta^c_j))\}$, we obtain the coefficient vectors $\mathbf{a}$ and $\boldsymbol{\lambda}$ for our RBF approximation (14) by forming and solving the linear system (17).

4. Frechet derivatives

4.1. Basic relations

Define the residual $\vartheta(f;\omega)$, in the continuous domain representation of the unknown parameter $f(x,z)$, at a frequency ω, to be

$$\vartheta(f;\omega) = \mathbf{u}_{\text{data}}(\omega) - \mathcal{A}(f;\omega), \tag{20}$$

where the ith component of the measurement operator $\mathcal{A}$ (corresponding to the ith measurement) at the given frequency is $\mathcal{A}^i(f;\omega,\mathbf{r}^i) \equiv u_{sc}(\mathbf{r}^i,\omega;f)$ (as defined in (B.3)). Note that $\boldsymbol{\zeta} = (\text{Real}(\vartheta), \text{Imag}(\vartheta))^T$.

The Frechet derivative of the residual can thus be written as

$$\vartheta'(f)\delta f = \mathbf{v}, \tag{21}$$

where the ith component of $\mathbf{v}$ (corresponding to the ith receiver) is $v_i \equiv v(\mathbf{r}^{\mathbf{i}},\omega)$, with $v(\mathbf{r},\omega)$ being a solution of

$$\Delta v(\mathbf{r},\omega) + k^2_{\text{nom}} v(\mathbf{r},\omega) = -k^2_{\text{amb}}\delta f(\mathbf{r}) u(\mathbf{r},\omega), \tag{22}$$

where Δ is the Laplacian operator and k_{nom} is the nominal wave number at the present iterate.

Thus the solution for $v_i := v(\mathbf{r}^i,\omega)$ in the integral form would be

$$v(\mathbf{r}^i,\omega) = \int_\Omega g_B(\mathbf{r}^i,\mathbf{r}',\omega)\big(k^2_{\text{amb}}\delta f(\mathbf{r}')\big)u(\mathbf{r}',\omega)\,\mathrm{d}\mathbf{r}', \tag{23}$$

where $g_B(\mathbf{r}^i,\mathbf{r}',\omega)$ is the Green function corresponding to the current parameter estimate being the ambient.

Thus, considering the object representation (4), we will have

$$\delta f(\mathbf{r}) = \alpha H'_\rho[s(\mathbf{r})]\delta s(\mathbf{r}) + H_\rho[s(\mathbf{r})]\delta\alpha \tag{24}$$

where $H'_\rho[.]$ denotes the derivative of the limiting Heaviside function $H_\rho[.]$ defined below (as in [17]),

$$H_\rho(t) := \begin{cases} 0 & \text{if} \quad t < -\rho \\ \dfrac{1}{2}\left\{1 + \dfrac{t}{\rho} + \dfrac{1}{\pi}\sin\left(\dfrac{\pi t}{\rho}\right)\right\} & \text{if} \quad t \in [-\rho,\rho] \\ 1 & \text{if} \quad t > \rho. \end{cases} \tag{25}$$

Observing from equation (25) that the support of $H'_\rho[s(\mathbf{r})]$ is contained in $s^{-1}[-\rho,\rho]$, we can thus write equation (23) as

$$\begin{aligned} v(\mathbf{r}^i,\omega) = &\int_{s^{-1}[-\rho,\rho]} g_B(\mathbf{r}^i,\mathbf{r}',\omega)k^2_{\text{amb}}(\mathbf{r}',\omega)u(\mathbf{r}',\omega)\alpha H'_\rho[s(\mathbf{r}')]\delta s(\mathbf{r}')\,\mathrm{d}\mathbf{r}' \\ &+ \delta\alpha\int_\Omega g_B(\mathbf{r}^i,\mathbf{r}',\omega)k^2_{\text{amb}}(\mathbf{r}',\omega)u(\mathbf{r}',\omega)H_\rho[s(\mathbf{r}')]\,\mathrm{d}\mathbf{r}'. \end{aligned} \tag{26}$$

We mention that the choice of the Heaviside parameter ρ should be such that the interpolating function $s(\mathbf{r})$ should be a good approximation to a signed distance function in the 'tubular' region $s^{-1}[-\rho, \rho]$. In our work, as in [8], for a plane curve $\gamma(x, z) = 0$ such as in the two-dimensional problems under consideration, we can define the tube as consisting of all parallel curves $\gamma(x, z) = \varepsilon$ such that $|\varepsilon\kappa(x, z)| < 1$ for all values of $(x, z) \in \partial\Omega$, where $\kappa(x, z)$ is the curvature of the curve $\gamma(x, z) = 0$. This condition ensures both, that a parallel curve is regular, as well as that the normal vectors of the curve $\gamma(x, z) = 0$ coincide with those of a parallel curve $\gamma(x, z) = \varepsilon$ for all $(x, z) \in \partial\Omega$ [20, 21].

In the present work we solve the forward problem numerically by the method of moments with a pulse-basis point-matching decomposition of the scattering integral equation [18, 19] (the essential discretization steps have been mentioned in appendix B). Assume basis decompositions of the following forms for the parameter function $f(.)$ and the field $u(.)$:

$$f(\mathbf{r}) = \sum_{j=1}^{n} f_j \psi_j(\mathbf{r}), \qquad u(\mathbf{r}, \omega) = \sum_{j=1}^{n} u_j(\omega)\psi_j(\mathbf{r}), \tag{27}$$

where n is the number of pixels in the image, and, $\{\psi_j(\mathbf{r})\}$ is an appropriate basis set; in our case, we choose it to be the pulse-basis i.e., $\psi_j(\mathbf{r}) = 1$ for $\mathbf{r} \in$ pixel j and zero otherwise.

Assuming that a pulse basis discretization in a method of moments framework is suitable for the coverage of the area covered by $\delta f(\mathbf{r})$ in (23), it would follow that (26) too could be discretized via the same pulse basis.

Thus, in a pulse-basis discretization of $\delta s(\mathbf{r})$ and $u(\mathbf{r}', \omega)$, we write the discrete approximation of equation (26) as

$$v_i = \sum_{j:(\mathbf{r}_j \in s^{-1}[-\rho,\rho])} G_B(i, j) u_j \{\alpha H'_\rho[s_j]\}\delta s_j + \delta\alpha \sum_j G_B(i, j) u_j H_\rho[s_j] \tag{28}$$

where $s_j = s(\mathbf{r}_j)$, and

$$G_B(i, j) = \int_\Omega g_B(\mathbf{r}^i, \mathbf{r}', \omega) k^2_{\text{amb}}(\mathbf{r}', \omega)\psi_j(\mathbf{r}')\, \mathrm{d}\mathbf{r}', \tag{29}$$

where the ω dependence in $G_B(i, j)$ (on the left-hand side) has been suppressed for ease of notation.

Using the equivalence of the distorted-Born and Newton–Kantorovich formulations [22], denoting $\delta\vartheta_i := v_i$, we can write

$$\delta\vartheta_i = \sum_{j:(\mathbf{r}_j \in s^{-1}[-\rho,\rho])} \frac{\partial\vartheta_i}{\partial f_j}\{\alpha H'_\rho[s_j]\}\delta s_j + \sum_j \frac{\partial\vartheta_i}{\partial f_j} H_\rho[s_j]\delta\alpha \tag{30}$$

where relations for $\frac{\partial\vartheta_i}{\partial f_j}$ are in appendix B.

Thus it is now left to evaluate the variations δs_j of the level-set function $s(.)$ with respect to variations in the RBF centers and corresponding unit normals.

4.2. Shape derivatives

We now recall from (14) that

$$s(\mathbf{r}) = \sum_{l=1}^{L} a_l p_l(\mathbf{r}) + \sum_{j=1}^{m} \left[c_j \Phi\left(\mathbf{r} - \mathbf{r}^c_j\right) - d_j \Psi_j\left(\mathbf{r} - \mathbf{r}^c_j\right)\right], \tag{31}$$

where $\Psi_j(.) \equiv (D_{n_j}\Phi)(.)$, and

$$\Psi_j\left(\mathbf{r} - \mathbf{r}^c_j\right) \equiv (\nabla\phi)\left(\mathbf{r} - \mathbf{r}^c_j\right) \cdot \mathbf{n}_j = \phi_x\left(\mathbf{r} - \mathbf{r}^c_j\right)\cos\theta^c_j + \phi_z\left(\mathbf{r} - \mathbf{r}^c_j\right)\sin\theta^c_j. \tag{32}$$

Evaluating the first variation of s, we have

$$\delta s(\mathbf{r}) = \sum_{l=1}^{L} \delta a_l p_l(\mathbf{r}) + \sum_{j=1}^{m} \big[c_j \delta\Phi\big(\mathbf{r}-\mathbf{r}_j^c\big) + \delta c_j \Phi\big(\mathbf{r}-\mathbf{r}_j^c\big) - d_j \delta\Psi_j\big(\mathbf{r}-\mathbf{r}_j^c\big) - \delta d_j \Psi_j\big(\mathbf{r}-\mathbf{r}_j^c\big)\big] \tag{33}$$

where, further,

$$\delta\Phi\big(\mathbf{r}-\mathbf{r}_j^c\big) = -\Phi_x\big(\mathbf{r}-\mathbf{r}_j^c\big)\delta x_j^c - \Phi_z\big(\mathbf{r}-\mathbf{r}_j^c\big)\delta z_j^c \tag{34}$$

and similarly,

$$\delta\Psi_j\big(\mathbf{r}-\mathbf{r}_j^c\big) = \big[-\Phi_{xx}\big(\mathbf{r}-\mathbf{r}_j^c\big)\cos\theta_j^c - \Phi_{zx}\big(\mathbf{r}-\mathbf{r}_j^c\big)\sin\theta_j^c\big]\delta x_j^c \tag{35}$$

$$+ \big[-\Phi_{xz}\big(\mathbf{r}-\mathbf{r}_j^c\big)\cos\theta_j^c - \Phi_{zz}\big(\mathbf{r}-\mathbf{r}_j^c\big)\sin\theta_j^c\big]\delta z_j^c \tag{36}$$

$$+ \big[-\Phi_{x}\big(\mathbf{r}-\mathbf{r}_j^c\big)\sin\theta_j^c + \Phi_{z}\big(\mathbf{r}-\mathbf{r}_j^c\big)\big]\delta\theta_j^c. \tag{37}$$

Hence, in (33), it only remains to evaluate δc_j and δd_j in terms of the variations of the RBF centers and normals, i.e., to evaluate $\delta\boldsymbol{\lambda}$ and $\delta\mathbf{a}$. To do this, we take the first variation of the interpolation system of equations (17) to obtain

$$\begin{pmatrix} \delta A & \delta P \\ \delta P^T & \mathbf{0} \end{pmatrix}\begin{pmatrix} \boldsymbol{\lambda} \\ \mathbf{a} \end{pmatrix} + \begin{pmatrix} A & P \\ P^T & \mathbf{0} \end{pmatrix}\begin{pmatrix} \delta\boldsymbol{\lambda} \\ \delta\mathbf{a} \end{pmatrix} = \mathbf{0}. \tag{38}$$

Hence we obtain,

$$\begin{pmatrix} \delta\boldsymbol{\lambda} \\ \delta\mathbf{a} \end{pmatrix} = -\begin{pmatrix} A & P \\ P^T & \mathbf{0} \end{pmatrix}^{-1}\begin{pmatrix} (\delta A)\boldsymbol{\lambda} + (\delta P)\mathbf{a} \\ (\delta P^T)\boldsymbol{\lambda} \end{pmatrix}. \tag{39}$$

We now make the following definitions:

$$(\delta A)\boldsymbol{\lambda} \equiv B\begin{pmatrix} \mathbf{x^c} \\ \mathbf{z^c} \\ \theta^{\mathbf{c}} \end{pmatrix}, \qquad (\delta P)\mathbf{a} \equiv P_a\begin{pmatrix} \mathbf{x^c} \\ \mathbf{z^c} \\ \theta^{\mathbf{c}} \end{pmatrix}, \qquad (\delta P^T)\boldsymbol{\lambda} \equiv P_\lambda\begin{pmatrix} \mathbf{x^c} \\ \mathbf{z^c} \\ \theta^{\mathbf{c}} \end{pmatrix}, \tag{40}$$

where the functional forms (explicitly given in appendix A) for B, P_a and P_λ are obtained by appropriate rearrangement of respective left-hand sides in the expressions above.

Thus, denoting $\tilde{A} \equiv \left(\begin{smallmatrix} A & P \\ P^T & \mathbf{0} \end{smallmatrix}\right)$ and $\tilde{B} \equiv \left(\begin{smallmatrix} B+P_a \\ P_\lambda \end{smallmatrix}\right)$, we obtain

$$\begin{pmatrix} \delta\boldsymbol{\lambda} \\ \delta\mathbf{a} \end{pmatrix} = -\tilde{A}^{-1}\tilde{B}\begin{pmatrix} \mathbf{x^c} \\ \mathbf{z^c} \\ \theta^{\mathbf{c}} \end{pmatrix}. \tag{41}$$

Thus, we can write the first variation expression (33) in compact notation, as

$$\delta\mathbf{s} = \mathbf{J}_s\begin{pmatrix} \mathbf{x^c} \\ \mathbf{z^c} \\ \theta^{\mathbf{c}} \end{pmatrix}, \tag{42}$$

where

$$\mathbf{J}_s = F - (R[\tilde{A}^{-1}]_a + \boldsymbol{\Phi}[\tilde{A}^{-1}]_c - \boldsymbol{\Psi}[\tilde{A}^{-1}]_d)\tilde{B} \tag{43}$$

where

(1) $\mathbf{s}$ is the vector of values of $s(\mathbf{r})$ at the required (N_T number of) points.

(2) $\mathbf{\Phi}$ (resp. $\mathbf{\Psi}$) is the $N_T \times m$ matrix with $\mathbf{\Phi}_{ij} = \Phi(\mathbf{r}_i - \mathbf{r}_j^c)$ (resp. $\mathbf{\Psi}_{ij} = \Psi_j(\mathbf{r}_i - \mathbf{r}_j^c)$), where $\mathbf{r}_i$ is the ith point at which the value of δs needs to be calculated. Similarly the derivative matrices $\mathbf{\Phi}_x$, $\mathbf{\Phi}_z$, $\mathbf{\Phi}_{xx}$, $\mathbf{\Phi}_{xz}$ and $\mathbf{\Phi}_{zz}$ can be defined.
(3) R is an $N_T \times L$ matrix with $R_{nl} = p_l(\mathbf{r}_n)$.
(4) $[\tilde{A}^{-1}]_a$ (resp. $[\tilde{A}^{-1}]_c$ and $[\tilde{A}^{-1}]_d$) corresponds to the last L rows (resp. rows 1 to m and $m+1$ to $2m$) of $\tilde{A}^{-1}$.
(5) $F = [F^x F^z F^\theta]$, with

$$F^x = -\mathbf{\Phi}_x \Lambda(\mathbf{c}) + [\mathbf{\Phi}_{xx} \Lambda(\cos\boldsymbol{\theta}^c) + \mathbf{\Phi}_{zx} \Lambda(\sin\boldsymbol{\theta}^c)]\Lambda(\mathbf{d}) \tag{44}$$

$$F^z = -\mathbf{\Phi}_z \Lambda(\mathbf{c}) + [\mathbf{\Phi}_{xz} \Lambda(\cos\boldsymbol{\theta}^c) + \mathbf{\Phi}_{zz} \Lambda(\sin\boldsymbol{\theta}^c)]\Lambda(\mathbf{d}) \tag{45}$$

$$F^\theta = [\mathbf{\Phi}_x \Lambda(\sin\boldsymbol{\theta}^c) - \mathbf{\Phi}_z \Lambda(\cos\boldsymbol{\theta}^c)]\Lambda(\mathbf{d}), \tag{46}$$

where $\Lambda(\mathbf{v}) \equiv \mathrm{diag}(v_1, \ldots, v_m)$ for some vector $\mathbf{v}$.

4.3. Overall frechet derivative

In matrix notation, the Frechet derivative in (30) can now be written as

$$\delta\boldsymbol{\vartheta} = \mathbf{J}_f \mathbf{J}_s \begin{pmatrix} \delta\mathbf{x}^\mathbf{c} \\ \delta\mathbf{z}^\mathbf{c} \\ \delta\theta^\mathbf{c} \end{pmatrix} + \mathbf{J}_\alpha \delta\alpha, \tag{47}$$

where $\delta\boldsymbol{\vartheta}$ is the first variation of the (complex) M-dimensional measurement vector $\boldsymbol{\vartheta}$, $\mathbf{J}_f$ is the $M \times N_T$ matrix with $[\mathbf{J}_f]_{ij} = \frac{\partial\vartheta_i}{\partial f_j}\{\alpha H'_\rho[s_j]\}$ and $\mathbf{J}_\alpha$ is the M-dimensional column vector with $[\mathbf{J}_\alpha]_i = \sum_j \frac{\partial\vartheta_i}{\partial f_j} H_\rho[s_j]$. Thus,

$$\delta\boldsymbol{\vartheta} = \mathbf{J}_C \begin{pmatrix} \delta\alpha \\ \delta\mathbf{x}^\mathbf{c} \\ \delta\mathbf{z}^\mathbf{c} \\ \delta\theta^\mathbf{c} \end{pmatrix} \tag{48}$$

where

$$\mathbf{J}_C = (\mathbf{J}_\alpha \quad \mathbf{J}_f \mathbf{J}_s). \tag{49}$$

5. Reconstruction scheme

5.1. Damped Tikhonov regularization based Gauss–Newton scheme

Recall from section 2 that the approximate tomographic problem to be solved is the minimum **c**-norm problem equation (7). To solve this problem, a scheme based upon an iteratively regularized Gauss–Newton approximation is utilized [8, 23, 24]. The multi-frequency GPR tomography problem under consideration in this work has an almost rank-deficient Jacobian matrix $\mathbf{J}(\mathbf{h})$ at the solution point of $\boldsymbol{\zeta}(\mathbf{h}) \simeq 0$. Using iterated Tikhonov regularization, a stable solution may be found which greatly improves the condition of the problem and also the convergence rate over the Gauss–Newton method applied to the unregularized functional.

The generic Tikhonov regularized (with regularization parameter η) nonlinear least-squares problem (7) can be written as

$$\min_\mathbf{h} \tfrac{1}{2} \|\boldsymbol{\zeta}_{\mathrm{aug}}(\mathbf{h}; \eta)\|^2 \tag{50}$$

where

$$\zeta_{\text{aug}}(\mathbf{h};\eta) \equiv \begin{pmatrix} \zeta(\mathbf{h}) \\ \eta(\mathbf{h}-\mathbf{c}) \end{pmatrix}. \tag{51}$$

Basically, we are solving approximately a sequence of Tikhonov regularized nonlinear least squares problems ($\min_{\mathbf{h}}\zeta_{\text{aug}}(\mathbf{h};\eta_t)$) for a fixed center $\mathbf{c}$ and a sequence of decreasing regularization parameters η_t. The approximate solution $\mathbf{h}(\eta_t)$ of one such subproblem is taken as the starting point of the next subproblem with regularization parameter $\eta_{t+1} < \eta_t$. The Gauss–Newton method is used to compute an approximate solution for this kind of subproblem. In the remainder of the paper, for ease of notation, we use η instead of η_t.

In practical applications, numerical experience allows us to take the approximate solution of a subproblem to be the minimum of the linear-residual approximation to that objective function[4]. Recalling that the Gauss–Newton method goes to the minimum of such a quadratic objective function in one iteration, we use a computationally inexpensive approach of checking at each iteration whether to reduce the regularization parameter or not, depending on whether or not, at that iterate, the first-order model is a good enough approximation of the actual residual. If the step length is 1, that is, a full step has been taken, it is assumed that the first-order model is good enough. It is important to note that by decreasing η, what is actually done is to change the optimization problem to one that is less smooth (i.e., to a more rapidly varying objective functional).

The regularization parameter η is a smoothing factor which should be larger than the noise, and a larger η gives an easier optimization problem to solve. A large (resp. small) η gives a solution close to (resp. away from) '$\mathbf{c}$'. As is often observed in nonlinear regularization problems, too small a η can result in the Gauss–Newton method not converging. Hence, it is important to start the algorithm with a large η, so that the iterates do not get driven too far from '$\mathbf{c}$' initially. During iterations η should be decreased (never increased though for that $\mathbf{c}$) in order to find lower minima. Observe that this will lead to a solution further away from '$\mathbf{c}$'.

To solve this problem, an iterative scheme based upon the Gauss–Newton approximation solves, at the current iterate $\mathbf{h}$,

$$\min_{\mathbf{p}} \left\| \begin{pmatrix} \mathbf{J}(\mathbf{h})\mathbf{p} + \zeta(\mathbf{h}) \\ \eta(\mathbf{h}-\mathbf{c}+\mathbf{p}) \end{pmatrix} \right\|^2 \tag{52}$$

where the $M \times N$ matrix $\mathbf{J}(\mathbf{h})$ is the Jacobian matrix of the functional $\zeta(\mathbf{h})$ with respect to $\mathbf{h}$, defined via a Taylor series expansion of the form

$$\zeta(\mathbf{h}+\mathbf{p}) = \zeta(\mathbf{h}) + \mathbf{J}(\mathbf{h})\mathbf{p} + \mathcal{O}(\|\mathbf{p}\|^2), \tag{53}$$

where the Jacobian $\mathbf{J}$ is easily calculated from the matrix $\mathbf{J}_C$ (defined in (49)) by recalling that $\zeta = (\text{Real}(\vartheta), \text{Imag}(\vartheta))^T$, and is given by

$$\mathbf{J} = \begin{pmatrix} \text{Re}(\mathbf{J}_\alpha) & \text{Im}(-\mathbf{J}_\alpha) & \text{Re}(\mathbf{J}_f\mathbf{J}_s) \\ \text{Im}(\mathbf{J}_\alpha) & \text{Re}(\mathbf{J}_\alpha) & \text{Im}(\mathbf{J}_f\mathbf{J}_s) \end{pmatrix}. \tag{54}$$

The next iterate is given by

$$\mathbf{h}^{k+1} = \mathbf{h}^k + \beta_k \mathbf{p}^k, \tag{55}$$

where the step length β_k is chosen via line-search such that the objective functional is sufficiently reduced. The search direction $\mathbf{p}^k$ computed from (52) can be written as

$$\mathbf{p}^k = -\mathbf{B}(\mathbf{h}^k) \begin{pmatrix} \zeta(\mathbf{h}^k) \\ \mathbf{h}^k - \mathbf{c} \end{pmatrix}, \tag{56}$$

[4] Note that the objective function is proportional to the squared norm of the residual.

where

$$\mathbf{B}_k \equiv \mathbf{B}(\mathbf{h}^k) = \left(\left(\mathbf{J}_k^T\mathbf{J}_k + \eta^2\mathbf{I}\right)^{-1}\mathbf{J}_k^T \;\middle|\; \eta^2\left(\mathbf{J}_k^T\mathbf{J}_k + \eta^2\mathbf{I}\right)^{-1}\right). \tag{57}$$

We do not explicitly form the product $\mathbf{J}_k^T\mathbf{J}_k$ in the computation of the matrix $\mathbf{B}_k$ for reasons of numerical stability; it is computed via the singular value decomposition of $\mathbf{J}_k$.

The termination criterion we have used is a relative one, i.e., we measure 'how much' of the residual remains to minimize. The relative criterion is defined as

$$\epsilon_{\text{rel}} = \frac{\|\mathcal{P}_{J\text{aug}}\|}{\|\zeta_{\text{aug}}\|}, \tag{58}$$

where $\mathcal{P}_{J\text{aug}}$ is the orthogonal projection onto the range space of $\mathbf{J}_{\text{aug}}$, and

$$\mathbf{J}_{\text{aug}} = \begin{pmatrix} \mathbf{J}(\mathbf{h}) \\ \eta\mathbf{I}_N \end{pmatrix}. \tag{59}$$

Termination of the nonlinear recursive scheme is set as satisfaction of the criterion $\epsilon_{\text{rel}} < \text{tol}$ for some tolerance limit tol or the iterates staying stable.

5.2. Initialization

As in [8], the initialization of the recursive scheme is done by estimating a circular homogeneous object that best generates the measured data under the Born-approximation. Since the linearized scattering equation may not truly represent the scattering process, a constraint is applied on the maximum magnitude of reconstructed values of object inhomogeneity parameters, to ensure that the object is within the validity of the Born approximation; in the present work, we have set $|\alpha| < 0.6$ for the starting estimate. Define

$$\tilde{\mathbf{h}} = \begin{pmatrix} \text{Re}(\alpha) \\ \text{Im}(\alpha) \\ x_{\text{center}} \\ z_{\text{center}} \\ R_{\text{circle}} \end{pmatrix} \tag{60}$$

with $(x_{\text{center}}, z_{\text{center}}) \equiv \mathbf{r}_{\text{center}}$ and R_{circle} being the center coordinates and radius of the circular object, respectively.

Hence an estimate of the 'best-fit' circular object within the Born approximation can be obtained as

$$\min_{\tilde{\mathbf{h}}\in\mathbf{D}} \|\zeta^{\text{Born}}(\tilde{\mathbf{h}})\|^2, \tag{61}$$

where $\mathbf{D}$ represents assumed box bounds for the various unknowns

$$\zeta^{\text{Born}}(\tilde{\mathbf{h}}) = \begin{pmatrix} \text{Real}(\mathbf{u_{data}} - \mathcal{A}^{\text{Born}}(\tilde{\mathbf{h}})) \\ \text{Imag}(\mathbf{u_{data}} - \mathcal{A}^{\text{Born}}(\tilde{\mathbf{h}})) \end{pmatrix} \tag{62}$$

where, $\mathcal{A}^{\text{Born}}(\tilde{\mathbf{h}})$ is the scattered field under the Born approximation, and is obtained from $\mathcal{A}(\tilde{\mathbf{h}})$ (as defined after equation (7)) by replacing $u(\mathbf{r}', \omega, \tilde{\mathbf{h}})$ by $u_{\text{amb}}(\mathbf{r}', \omega)$ in the integrand, and noting that the level-set function for an object with a circular boundary can be evaluated as

$$\gamma(\mathbf{r}', \tilde{\mathbf{h}}) = R_{\text{circle}} - \|\mathbf{r}' - \mathbf{r}_{\text{center}}\|. \tag{63}$$

The approximation to the Heaviside function used for the evaluation of this first estimate is $H[.] \simeq H_\rho[.]$, where ρ has been set as the method-of-moments' (MoM's) grid-discretization interval $\mathrm{d}x$ for the initialization step to ensure a gradual slope. The initial RBF centers of

the full nonlinear scheme are distributed along the perimeter of this initial circular object. Typically, in our initial estimate, we set the imaginary part of the inhomogeneity parameter α to zero.

The overall algorithm is provided below.

I *Initialization*
(**a**) Estimate $\mathbf{h}^0$, the 'best-fit' circular object within the Born approximation according to (61).
(**b**) $\mathbf{c} := \mathbf{h}^0$, η set at a suitable 'large' value.
II *Reconstruction phase*
For $k = 1, 2, \ldots,$ till $\epsilon_{\text{rel}} <$ tol or residual is unchanging for many past k
(**a**) Estimate the Heaviside approximation parameter, ρ, as $\min(\mathrm{d}x, \varepsilon_{\max})$, where $\varepsilon_{\max} = \max\{\varepsilon; |\varepsilon\kappa(x, z)| < 1$ for all values of $(x, z) \in \partial\Omega\}$ and $\mathrm{d}x$ is the MoM grid-discretization interval.
(**b**) Evaluate the Jacobian $\mathbf{J}(\mathbf{h}^k)$ using (54).
(**c**) Solve (52) for $\mathbf{p}^k$.
(**d**) Do a line search to find β_k.
(**e**) If $\beta_k \simeq 1$, then, $\eta := \eta/q$, for a suitable choice of $q > 1$(we chose $q = 2$).
(**f**) $\mathbf{h}^{k+1} = \mathbf{h}^k + \beta_k \mathbf{p}^k$.

6. Numerical studies

Numerical studies have been carried out on the simultaneous electrical parameter and shape reconstruction problem of single and double object phantoms of small dielectric mine-like objects of different shapes for various noise conditions. Scattered data at multiple-frequencies (0.7, 0.9, 1.1, 1.3 GHz) and multiple-angle plane wave incidence (15 angles in $[-\pi/3, \pi/3]$) is used in our studies. Data sets have been simulated by adding Gaussian random noise of different variance to the exact data. In these studies, the scattered-field data are collected on a line 10 cm above the ground, and at each frequency, 120 data points are considered from $x = -24$ cm to $x = 24$ cm. The subsurface reconstruction domain considered is 16 cm $\times$ 16 cm ($x = -8$ cm,. . ., 8 cm and $z = -0.4$ cm, . . . , − 16.4 cm). In the method of moments discretization of the reconstruction domain, we use a grid of 40×40.

The test cases are specified by some combination of shapes, number of objects and material compositions. Phantom P1 is a single object with a concavity and material parameters as in composition B1 (as in table 1), P2 is a single near-circular object with composition B1 and P3 is a double-rectangle phantom with composition B2. Data are simulated with various noise levels, denoted by N1 and N2, formed by adding Gaussian noise of zero mean and standard deviation of 0.1 and 0.2 times the maximum absolute value of the exact data set. The signal-to-noise ratio (SNR) values for the data sets P1N1, P1N2, P2N1, P2N2, P3N1 and P3N2 are 26.570 39 dB, 12.912 51 dB, 28.233 47 dB, 13.993 49 dB, 29.081 76 dB and 15.212 41 dB, respectively. In the present work, without loss of conceptual generality, we have considered phantoms where all the constituent objects (in a phantom) have the same electrical parameter; using level-set based representations for multiple parameter values such as those mentioned in [25], the conceptual extension to those cases follows.

In the present work, for phantoms P1 and P2, for generation of the shapes to simulate the measurement data, B-splines of order 4 and 8 distinct control points have been used [8, 26]. The double rectangular phantom P3 on the other hand is generated as the intersecting region

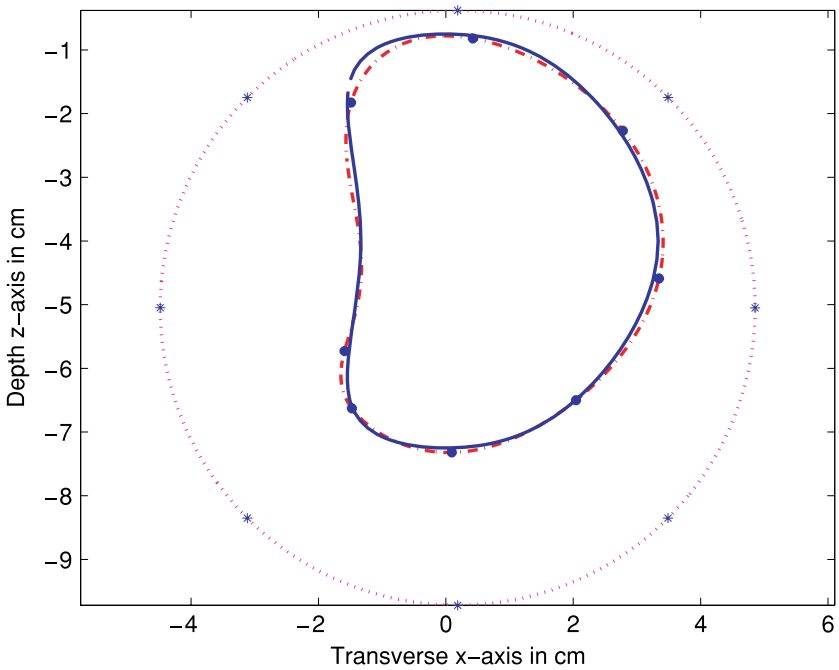

Figure 1. Phantom P1N1 (Data SNR = 26.57039 dB); actual shape: solid line, reconstructed shape: dot-dashed line, first estimate: dotted line; '*': RBF-center reconstructed $f = 1.201496 - \mathrm{i}\,0.031046$; actual $f = 1.2221 - \mathrm{i}\,0.02667$.

Table 1. Test case material settings.

Notation	Ambient (ϵ_r, $\tan\delta$)	Object (ϵ_r, $\tan\delta$, f)
B1	Wet sand (4.5, 0.03)	(10, 0.01797, 1.2221 − i0.02667)
B2	Dry sand, (2.55, 0.0282)	(4.24, 0.0636, 0.6644 + i0.0588)

of the component straight lines. This ensures that our reconstruction shape model is different from that used to generate the actual shapes.

The reconstructions are demonstrated in figures 1–6. In the figures the stars indicate the locations of the RBF centers. As is commonly observed, the number of centers can be considered as an implicit regularization parameter in the solution of the reconstruction problem; however, for the numerical studies in this work we fix this *a priori* and regularize the resultant almost rank-deficient problem in the iterative regularization scheme described in the previous section. We picked the least number of centers that yielded closed boundary and parallel curves for objects of similar size as the actual test objects. In our work we used 8 centers for the single phantoms and 9 centers for the double phantom.

The single object reconstructions show good reconstructions of the shape and $\mathrm{Re}(\alpha)$ and most of the time also for $\mathrm{Im}(\alpha)$. For these objects, the results are seen to be comparable to those in [8]; even though that in our present work, the reconstruction shape (RBF) basis is different from the shape generation (B-spline) basis. In addition, in the computations, the fact

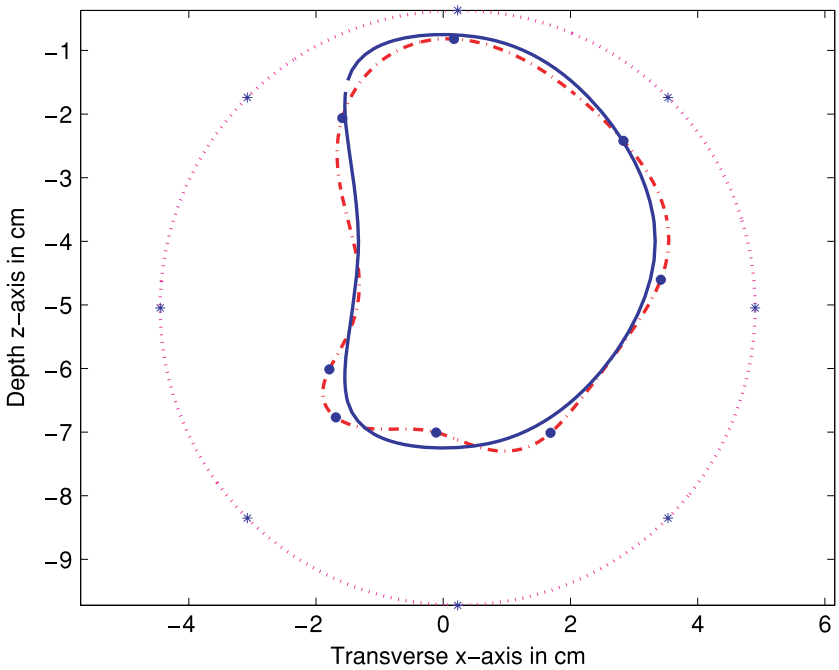

Figure 2. Phantom P1N2 (Data SNR = 12.91251 dB); actual shape: solid line, reconstructed shape: dot-dashed line, first estimate: dotted line; '*': RBF-center reconstructed $f = 1.18987 - \mathrm{i}\,0.026320$; actual $f = 1.2221 - \mathrm{i}\,0.02667$.

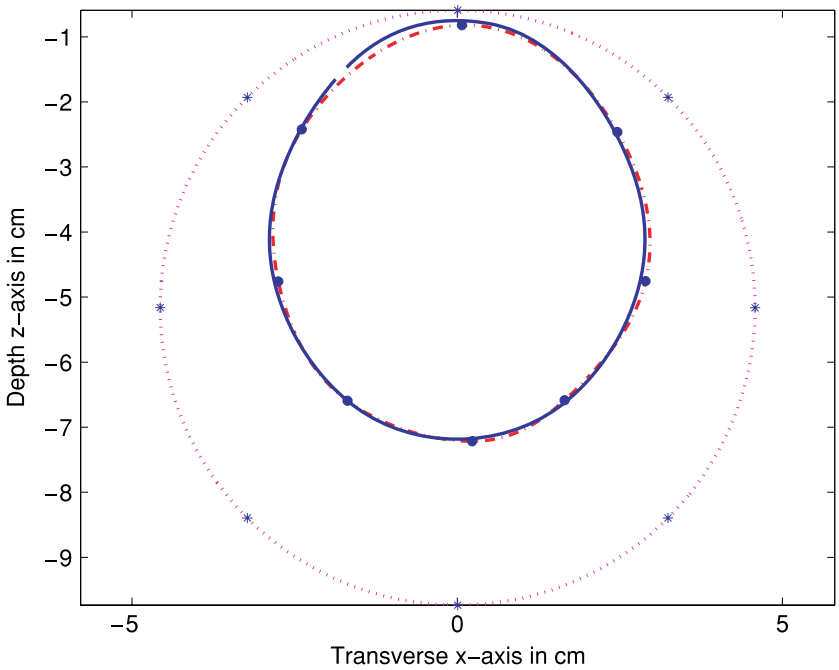

Figure 3. Phantom P2N1 (Data SNR = 28.23347 dB); actual shape: solid line, reconstructed shape: dot-dashed line, first estimate: dotted line; '*': RBF-center reconstructed $f = 1.22015 - \mathrm{i}\,0.027308$; actual $f = 1.2221 - \mathrm{i}\,0.02667$.

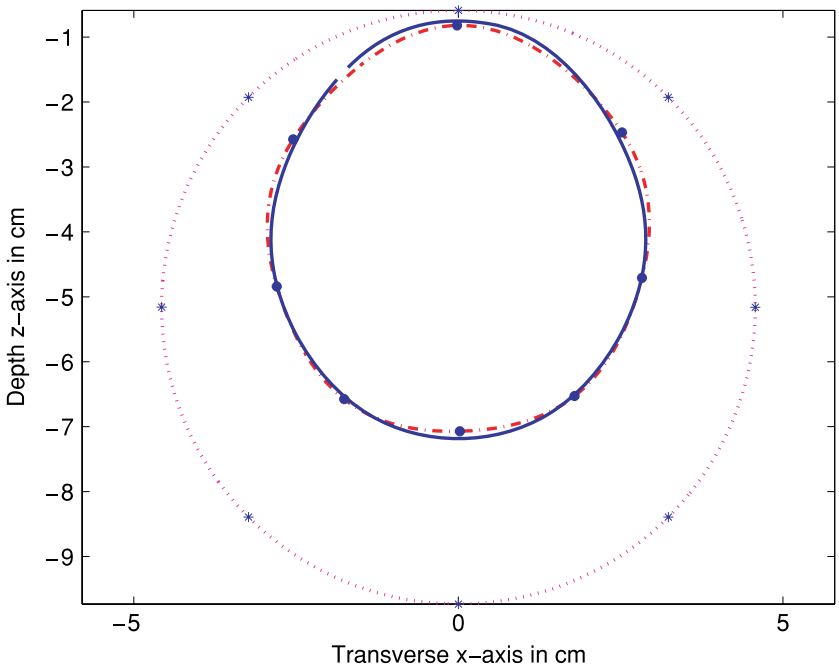

Figure 4. Phantom P2N2 (Data SNR = 13.99349 dB); actual shape: solid line, reconstructed shape: dot-dashed line, first estimate: dotted line; '*': RBF-center reconstructed $f = 1.23887 - \mathrm{i}\,0.012299$; actual $f = 1.2221 - \mathrm{i}\,0.02667$.

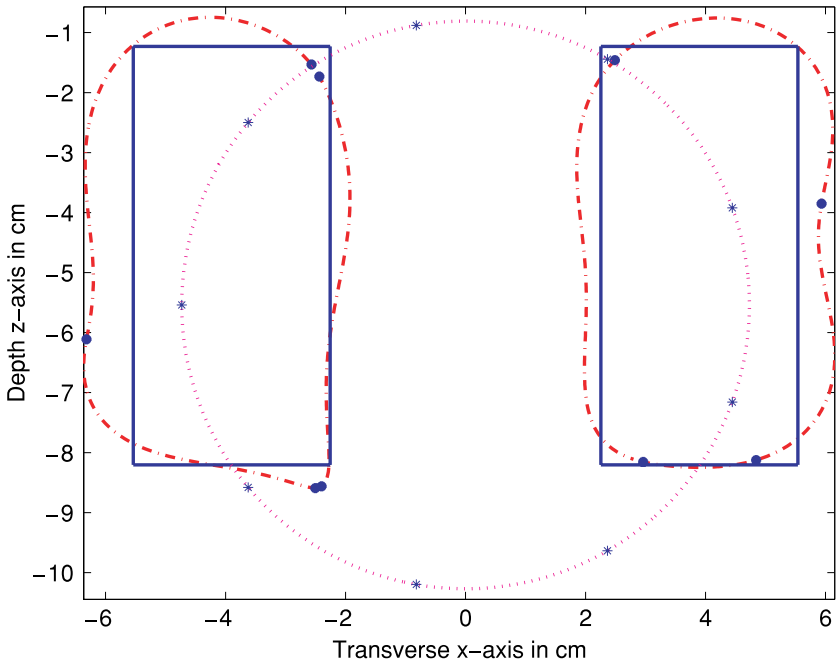

Figure 5. Phantom P3N1 (Data SNR = 29.08176 dB); actual shape: solid line, reconstructed shape: dot-dashed line, first estimate: dotted line; '*': RBF-center reconstructed $f = 0.55816 + \mathrm{i}\,0.032\,33$; actual $f = 0.6644 + \mathrm{i}\,0.0588$.

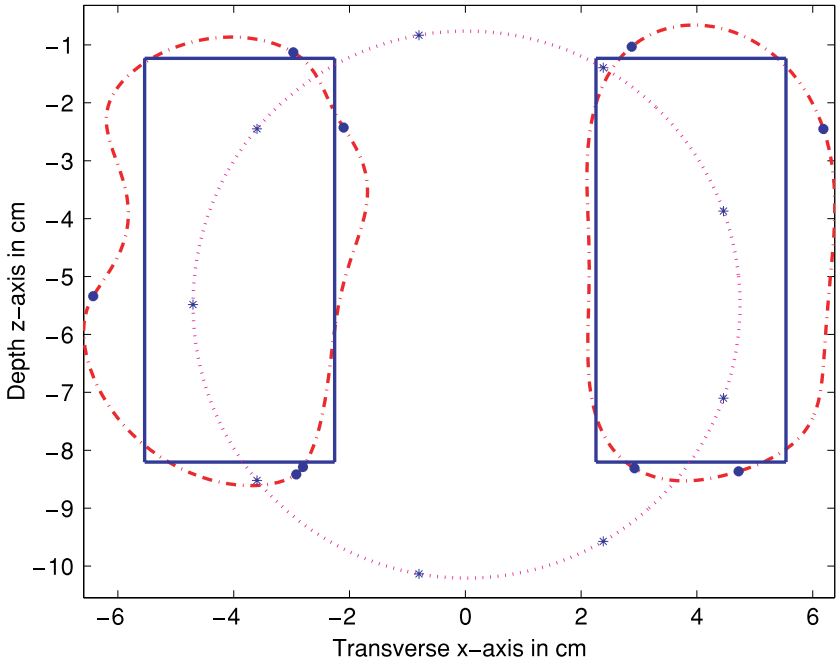

Figure 6. Phantom P3N2 (Data SNR = 15.21241 dB); actual shape: solid line, reconstructed shape: dot-dashed line, first estimate: dotted line; '*': RBF-center reconstructed $f = 0.536946 + \mathrm{i}\,0.014\,6560$; actual $f = 0.6644 + \mathrm{i}\,0.0588$.

that the RBF models the signed-distance-function eliminates the intermediate steps needed for an explicit reconstruction scheme to find the interior and exterior of the object of interest.

We are actually solving an interpolation problem in which the values of the level-set function and its directional derivative (along the normal) are specified; hence by problem statement itself the centers lie on the boundary curve. We point out though that the RBF model is an approximation of the actual signed-distance-function which in general is more accurate when we are closer to the boundary than farther away. At the points of interpolation (the RBF centers), the RBF model is naturally exact in value and in directional derivative.

The topology-changing capability and robustness of the present scheme is demonstrated in the reconstructions of phantom P3 starting from a first estimate that is a single object. In order to better visualize the topological changing process in our test cases, we have shown reconstruction sequences for the double phantoms in figures 7 and 8. We note that in addition to being a good test of the method for non-smooth boundaries, the rectangular double phantom lends itself to very exact scattered field calculations for data generation since the area coverage of these objects by the pulse basis elements is complete[5].

Termination of the reconstructions was set as either at the satisfaction of $\epsilon_{\mathrm{rel}} < 0.01$ or when the residual error consistently increases. We obtained termination of the reconstruction algorithm in 16, 15, 19, 15, 45 and 54 iterations for P1N1, P1N2, P2N1, P2N2, P3N1 and P3N2, respectively. We observe that the reconstructions of the double phantom object are more difficult than the single phantom in that they take more iterations to converge and

[5] The MoM integrations are area integrations and the better the area coverage, the more accurate are the scattering solutions.

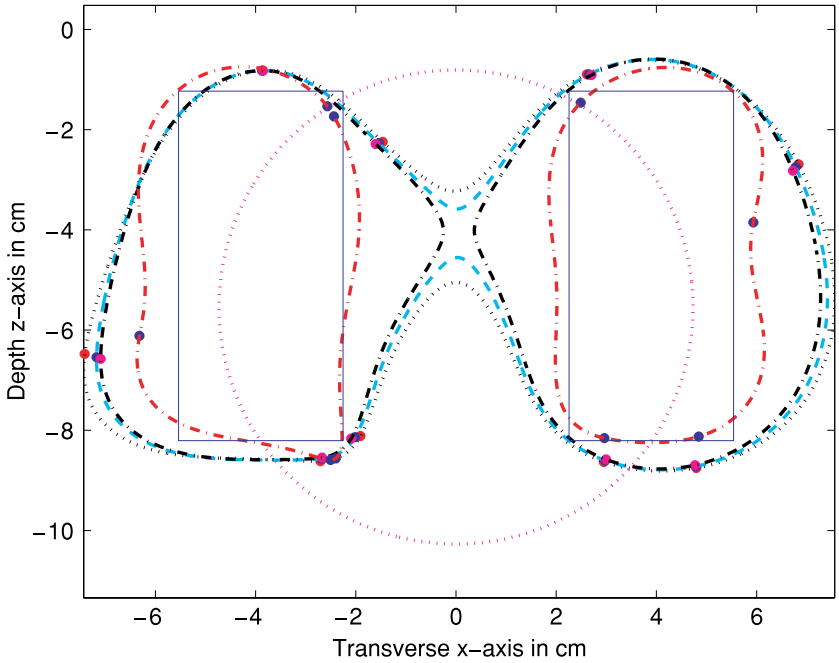

Figure 7. Reconstruction sequence for phantom P3N1 (Data SNR = 29.08176 dB) for iterates 10,11,12,45 (final); reconstructed shapes: dotted/dashed/dot-dashed lines, first estimate: circular dotted curve; actual shape: double rectangle in solid lines; '*': RBF-center.

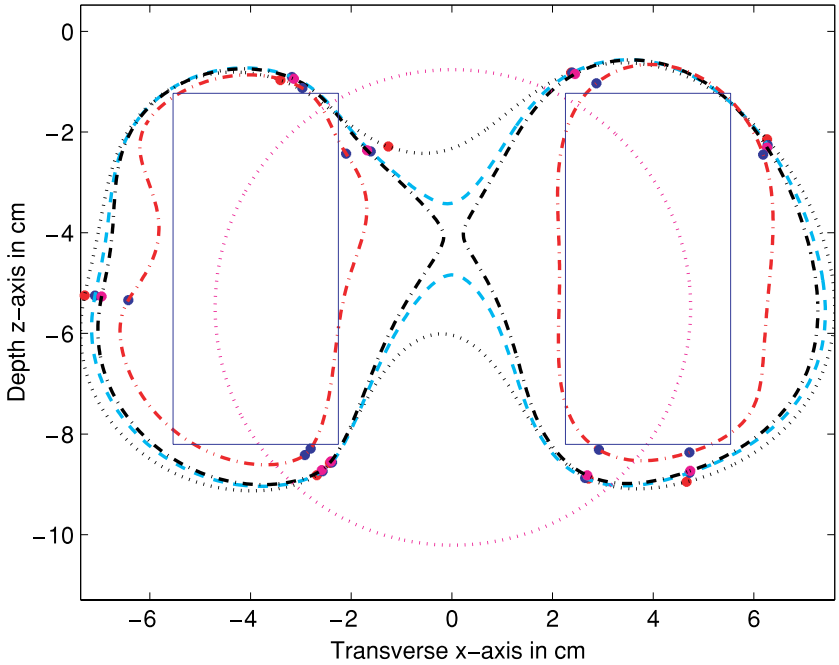

Figure 8. Reconstruction sequence for phantom P3N2 (Data SNR = 15.21241 dB) for iterates 25, 30, 31, 54 (final); reconstructed shapes: dotted/dashed/dot-dashed lines, first estimate: circular dotted curve; actual shape: double rectangle in solid lines; '*': RBF-center.

do not reconstruct the internal parameters as well as that for the single object; the case however demonstrates the robustness of the reconstruction scheme which separates out and well localizes the two objects.

7. Conclusions and further work

The present paper derives and provides a numerical validation of a novel simultaneous shape and electrical-parameter tomographic reconstruction scheme from scattered field data. The method uses a novel Hermite interpolation based implicit RBF representation of the boundary curve to *implicitly* describe the boundary in terms of a few on-curve points (the RBF centers) and the unit normals at the centers. The Frechet derivatives of the resulting objective functional w.r.t. the shape and electrical parameters are derived. The scheme is numerically validated with reconstructions of simulated mine-like objects. Some key observations and further constructions are

(1) As explained in the paper, the present implicit-representation scheme thus enjoys the advantages (and conceptually overcomes the respective disadvantages) of current implicit and explicit representation approaches by allowing for topological changes of the boundary curve, while having few unknowns respectively. This has been demonstrated by the reconstructions obtained for a double-object phantom starting from a single-object first estimate. In addition, the quality of reconstructions of the single-object phantoms is seen to be comparable to those obtained in [8], even though in our present work, the reconstruction shape (RBF) basis is different from the shape generation (B-spline) basis.
(2) In addition, the Hermite interpolation based RBF representation is a powerful and simple enough method to represent shapes in three dimensions, thus conceptually paving the way for the algorithm to be used in 3D. Of course, that would need a further investigation of methods to adaptively choose the appropriate number of centers, as well as sensitivity of the reconstructions to that number.
(3) In this work, we have used the triharmonic RBF basic function in our calculations. Different choices of RBFs need to be investigated especially to study their effect on conditioning of the interpolation matrix and thus on possible convergence aspects of the inversion iterations.

Appendix A

In this section we present the expressions for the matrices B, P_a and P_λ which have been defined as in (40) in section 4.

A.1. Evaluation of B

$$B\begin{pmatrix}\mathbf{x}^{\mathbf{c}}\\ \mathbf{z}^{\mathbf{c}}\\ \theta^{\mathbf{c}}\end{pmatrix} \equiv (\delta A)\boldsymbol{\lambda} = \begin{pmatrix}\delta A^{(11)}\mathbf{c} + \delta A^{(12)}\mathbf{d}\\ \delta A^{(21)}\mathbf{c} + \delta A^{(22)}\mathbf{d}\end{pmatrix}. \tag{A.1}$$

For $pq = 11, 12, 21, 22$, we denote $B^{pq} \equiv \left[B_x^{pq} B_z^{pq} B_\theta^{pq}\right]$, and

$$\delta A^{(pq)}\mathbf{v} \equiv B^{pq}\begin{pmatrix}\delta\mathbf{x}^{\mathbf{c}}\\ \delta\mathbf{z}^{\mathbf{c}}\\ \delta\theta^{\mathbf{c}}\end{pmatrix} = B_x^{pq}\delta\mathbf{x}^{\mathbf{c}} + B_z^{pq}\delta\mathbf{z}^{\mathbf{c}} + B_\theta^{pq}\delta\boldsymbol{\theta}^{c} \tag{A.2}$$

where $\mathbf{v} \equiv \mathbf{c}$ for $pq = 11, 21$, and $\mathbf{v} \equiv \mathbf{d}$ for $pq = 12, 22$.

We now briefly sketch the calculation of the various components of the matrix B. For the case $pq = 11$, $\mathbf{v} \equiv \mathbf{c}$, and

$$[\delta A^{11}\mathbf{c}]_k = \sum_l \delta A^{11}_{kl} c_l = \sum_l c_l\big[\Phi_x\big(\mathbf{r}^c_k - \mathbf{r}^c_l\big)\big(\delta x^c_k - \delta x^c_l\big) + \Phi_z\big(\mathbf{r}^c_k - \mathbf{r}^c_l\big)\big(\delta z^c_k - \delta z^c_l\big)\big]. \quad (A.3)$$

Define $\big[T^{pq}_x\big]_{kl} \equiv$ Coefficient of $v_l\big(\delta x^c_k - \delta x^c_l\big)$, $\big[T^{pq}_z\big]_{kl} \equiv$ coefficient of $v_l\big(\delta z^c_k - \delta z^c_l\big)$. Further for $\varsigma \in \{x, z, xx, xz, zz, xxx, xxz, xzz, zzz\}$, define the derivative matrices $\mathbf{\Phi}^c_\varsigma$ as $\big[\mathbf{\Phi}^c_\varsigma\big]_{kl} \equiv \Phi_\varsigma\big(\mathbf{r}^c_k - \mathbf{r}^c_l\big)$.

Thus, since $v_l = c_l$ for $pq = 11$, $T^{11}_x = \mathbf{\Phi}^c_x$, $T^{11}_z = \mathbf{\Phi}^c_z$. Hence, we obtain for $\eta \in \{x, z\}$, $B^{11}_\eta = \mathrm{diag}\big(T^{11}_\eta \mathbf{v}\big) - T^{11}_\eta \Lambda(\mathbf{v})$, and, $B^{11}_\theta = \mathbf{0}$. Thus

$$\delta A^{11}\mathbf{c} = B^{11}_x \delta\mathbf{x}^\mathbf{c} + B^{11}_z \delta\mathbf{z}^\mathbf{c}. \quad (A.4)$$

Proceeding similarly for the other cases of $pq = 12, 21, 22$, we obtain $B^{pq}_\eta = \mathrm{diag}\big(T^{pq}_\eta \mathbf{v}\big) - T^{pq}_\eta \Lambda(\mathbf{v})$. Further,

$$T^{12}_x = -\mathbf{\Phi}^c_{xx}\Lambda(\cos(\boldsymbol{\theta}^c)) - \mathbf{\Phi}^c_{zx}\Lambda(\sin(\boldsymbol{\theta}^c)) \quad (A.5)$$

$$T^{12}_z = -\mathbf{\Phi}^c_{xz}\Lambda(\cos(\boldsymbol{\theta}^c)) - \mathbf{\Phi}^c_{zz}\Lambda(\sin(\boldsymbol{\theta}^c)) \quad (A.6)$$

$$T^{12}_\theta = \mathbf{\Phi}^c_x\Lambda(\sin(\boldsymbol{\theta}^c)) - \mathbf{\Phi}^c_z\Lambda(\cos(\boldsymbol{\theta}^c)) \quad (A.7)$$

with $B^{12}_\theta = T^{12}_\theta \Lambda(\mathbf{d})$.

In the $pq = 21$ case

$$T^{21}_x = \Lambda(\cos(\boldsymbol{\theta}^c))\mathbf{\Phi}^c_{xx} + \Lambda(\sin(\boldsymbol{\theta}^c))\mathbf{\Phi}^c_{zx} \quad (A.8)$$

$$T^{21}_z = \Lambda(\cos(\boldsymbol{\theta}^c))\mathbf{\Phi}^c_{xz} + \Lambda(\sin(\boldsymbol{\theta}^c))\mathbf{\Phi}^c_{zz} \quad (A.9)$$

$$T^{21}_\theta = -\Lambda(\sin(\boldsymbol{\theta}^c))\mathbf{\Phi}^c_x + \Lambda(\cos(\boldsymbol{\theta}^c))\mathbf{\Phi}^c_z \quad (A.10)$$

with $B^{21}_\theta = \Lambda\big(T^{21}_\theta \mathbf{c}\big)$. In the $pq = 22$ case, we have

$$T^{22}_x = -[\Lambda(\cos(\boldsymbol{\theta}^c))\mathbf{\Phi}^c_{xxx}\Lambda(\cos(\boldsymbol{\theta}^c)) + \sin(\Theta)\cdot *\mathbf{\Phi}^c_{xxz} + \Lambda(\sin(\boldsymbol{\theta}^c))\mathbf{\Phi}^c_{xzz}\Lambda(\sin(\boldsymbol{\theta}^c))], \quad (A.11)$$

where $\Theta \equiv \boldsymbol{\theta}^c \otimes \mathbf{1}^T + \mathbf{1} \otimes \boldsymbol{\theta}^{cT}$, where $\mathbf{1} = (1 \ldots 1)^T$ is a length m column vector, $\otimes$ represents the Kronecker product and the '.$*$' is after the Matlab notation for elementwise multiplication. Also,

$$T^{22}_z = -\big[\Lambda(\cos(\boldsymbol{\theta}^c))\mathbf{\Phi}^c_{xxz}\Lambda(\cos(\boldsymbol{\theta}^c)) + \sin(\Theta)\cdot *\mathbf{\Phi}^c_{xzz} + \Lambda(\sin(\boldsymbol{\theta}^c))\mathbf{\Phi}^c_{zzz}\Lambda(\sin(\boldsymbol{\theta}^c))\big] \quad (A.12)$$

$$T^{22}_{\theta_l} = \Lambda(\cos\boldsymbol{\theta}^c)\mathbf{\Phi}^c_{xx}\Lambda(\sin\boldsymbol{\theta}^c) - \cos\Theta\cdot *\mathbf{\Phi}^c_{xz} - \Lambda(\sin\boldsymbol{\theta}^c)\mathbf{\Phi}^c_{zz}\Lambda(\cos\boldsymbol{\theta}^c)] \quad (A.13)$$

$$T^{22}_{\theta_k} = \Lambda(\sin\boldsymbol{\theta}^c)\mathbf{\Phi}^c_{xx}\Lambda(\cos\boldsymbol{\theta}^c) - \cos\Theta\cdot *\mathbf{\Phi}^c_{xz} - \Lambda(\cos\boldsymbol{\theta}^c)\mathbf{\Phi}^c_{zz}\Lambda(\sin\boldsymbol{\theta}^c)] \quad (A.14)$$

with

$$B^{22}_\theta = T^{22}_{\theta_l}\Lambda\big(\mathbf{d}\big) + \Lambda(T^{22}_{\theta_k}\mathbf{d}\big). \quad (A.15)$$

A.2. Evaluation of P_a

From (18) we can write the matrix P in the following block form:

$$P = \begin{pmatrix} P^{(1)} \\ P^{(2)} \end{pmatrix} \tag{A.16}$$

where $P^{(1)}$ and $P^{(2)}$ are $m \times L$ matrices with elements

$$P^{(1)}_{lj} = p^{(j)}(\mathbf{r}_l) \tag{A.17}$$

$$P^{(2)}_{lj} = \nabla p^{(j)}(\mathbf{r}_l) \cdot n_l = p^{(j)}_x(\mathbf{r}_l)\cos\theta^c_l + p^{(j)}_z(\mathbf{r}_l)\sin\theta^c_l. \tag{A.18}$$

Hence, we can write

$$(\delta P)\mathbf{a} \equiv \begin{pmatrix} \delta P^{(1)}\mathbf{a} \\ \delta P^{(2)}\mathbf{a} \end{pmatrix} = \begin{pmatrix} \sum_{j=1}^m a_j\left(q^{(1x)}_{lj}\delta x^c_l + q^{(1z)}_{lj}\delta z^c_l\right) \\ \sum_{j=1}^m a_j\left(q^{(2x)}_{lj}\delta x^c_l + q^{(2z)}_{lj}\delta z^c_l + q^{(2\theta)}_{lj}\delta\theta^c_l\right) \end{pmatrix} \tag{A.19}$$

where for $p \in \{1, 2\}$, and $w \in \{x, z, \theta\}$, $q^{pw}_{lj} \equiv$ coefficient of δw^c_l in $\delta P^{(p)}_{lj}$, i.e.,

$$q^{1x}_{lj} = p^{(j)}_x(\mathbf{r}^c_l), \qquad q^{1z}_{lj} = p^{(j)}_z(\mathbf{r}^c_l) \tag{A.20}$$

$$q^{2x}_{lj} = p^{(j)}_{xx}(\mathbf{r}^c_l)\cos\theta^c_l + p^{(j)}_{zx}(\mathbf{r}^c_l)\sin\theta^c_l \tag{A.21}$$

$$q^{2z}_{lj} = p^{(j)}_{xz}(\mathbf{r}^c_l)\cos\theta^c_l + p^{(j)}_{zz}(\mathbf{r}^c_l)\sin\theta^c_l \tag{A.22}$$

$$q^{2\theta}_{lj} = p^{(j)}_z(\mathbf{r}^c_l)\cos\theta^c_l - p^{(j)}_x(\mathbf{r}^c_l)\sin\theta^c_l. \tag{A.23}$$

Thus, in compact notation, we can write

$$(\delta P)\mathbf{a} = \begin{pmatrix} \Lambda(Q^{(1x)}\mathbf{a}) & \Lambda(Q^{(1z)}\mathbf{a}) & \mathbf{0} \\ \Lambda(Q^{(2x)}\mathbf{a}) & \Lambda(Q^{(2z)}\mathbf{a}) & \Lambda(Q^{(2\theta)}\mathbf{a}) \end{pmatrix} \begin{pmatrix} \mathbf{x^c} \\ \mathbf{z^c} \\ \theta^{\mathbf{c}} \end{pmatrix} \tag{A.24}$$

thus yielding P_a (recalling from (40) that $(\delta P)\mathbf{a} \equiv P_a\left(\begin{smallmatrix} \mathbf{x^c} \\ \mathbf{z^c} \\ \theta^{\mathbf{c}} \end{smallmatrix}\right)$).

A.3. Evaluation of P_λ

From (A.16) we have

$$(\delta P^T)\boldsymbol{\lambda} = (\delta(P^{(1)})^T\delta(P^{(2)})^T)\begin{pmatrix} \mathbf{c} \\ \mathbf{d} \end{pmatrix} = \delta(P^{(1)})^T\mathbf{c} + \delta(P^{(2)})^T\mathbf{d}. \tag{A.25}$$

Hence

$$[(\delta P^T)\boldsymbol{\lambda}]_j = \sum_{l=1}^L \left[\delta(P^{(1)})^T_{jl}c_l + \delta(P^{(2)})^T_{jl}d_l\right] \tag{A.26}$$

$$= \sum_{l=1}^L \left[\delta x^c_l\left(c_l q^{(1x)}_{lj} + d_l q^{(2x)}_{lj}\right) + \delta y^c_l\left(c_l q^{(1z)}_{lj} + d_l q^{(2z)}_{lj}\right) + \delta\theta^c_l d_l q^{(2\theta)}_{lj}\right]. \tag{A.27}$$

Hence, in compact notation,

$$(\delta P^T)\boldsymbol{\lambda} = P_\lambda \begin{pmatrix} \mathbf{x^c} \\ \mathbf{z^c} \\ \theta^{\mathbf{c}} \end{pmatrix} \tag{A.28}$$

where

$$P_\lambda = \{(Q^{(1x)})^T \Lambda(\mathbf{c}) + (Q^{(2x)})^T \Lambda(\mathbf{d})\}\{(Q^{(1z)})^T \Lambda(\mathbf{c}) + (Q^{(2z)})^T \Lambda(\mathbf{d})\}(Q^{(2\theta)})^T \Lambda(\mathbf{d}). \tag{A.29}$$

Appendix B

B.1. Method of moments based Jacobian and Hessian

The total field is written as the sum of an incident ambient component, $u_{\text{amb}}(\mathbf{r}, \omega)$, and a scattered component $u_{sc}(\mathbf{r}, \omega; f)$, as follows:

$$u(\mathbf{r}, \omega; f) = u_{\text{amb}}(\mathbf{r}, \omega) + u_{sc}(\mathbf{r}, \omega; f) \tag{B.1}$$

where

$$u_{\text{amb}}(\mathbf{r}, \omega) = \int_{V_s} g(\mathbf{r}, \mathbf{r}', \omega) j_n(\mathbf{r}')\, \mathrm{d}\mathbf{r}' \tag{B.2}$$

and

$$u_{sc}(\mathbf{r}, \omega; f) = \int_\Omega g(\mathbf{r}, \mathbf{r}', \omega)\big(k^2_{\text{amb}}(\mathbf{r}', \omega) f(\mathbf{r}')\big) u(\mathbf{r}', \omega)\, \mathrm{d}\mathbf{r}', \tag{B.3}$$

where V_s is the volume enclosing the source distribution and Ω is the object-domain volume. The Green function $g(\mathbf{r}, \mathbf{r}', \omega)$ is the outgoing-wave solution of the equation

$$\Delta g(\mathbf{r}, \mathbf{r}', \omega) + k^2_{\text{amb}}(\mathbf{r}, \omega) g(\mathbf{r}, \mathbf{r}', \omega) = -\delta(\mathbf{r} - \mathbf{r}'). \tag{B.4}$$

The half-space Green function has been chosen for this work [19, 27].

From section 4.1, we recall the basis decompositions (27) of the following forms for the parameter function $f(.)$ and the field $u(.)$:

$$f(\mathbf{r}) = \sum_{j=1}^{n} f_j \psi_j(\mathbf{r}), \qquad u(\mathbf{r}, \omega) = \sum_{j=1}^{n} u_j(\omega) \psi_j(\mathbf{r}), \tag{B.5}$$

where n is the number of pixels in the image, and, $\{\psi_j(\mathbf{r})\}$ is an appropriate basis set; in our case, we choose it to be the pulse basis i.e., $\psi_j(\mathbf{r}) = 1$ for $\mathbf{r} \in \text{pixel}\, j$ and zero otherwise.

Substituting (27) into (B.3), we get

$$u_{sc}(\mathbf{r}, \omega) = \sum_{j=1}^{n} f_j u_j(\mathbf{f}, \omega) o_j(\mathbf{r}, \omega) \tag{B.6}$$

where

$$o_j(\mathbf{r}, \omega) = \int_\Omega g(\mathbf{r}, \mathbf{r}', \omega) k^2_{\text{amb}}(\mathbf{r}', \omega) \psi_j(\mathbf{r}')\, \mathrm{d}\mathbf{r}'. \tag{B.7}$$

Considering a point-matching scheme [18], we obtain the expression for the field at a point $x = x_i$, from (B.6) and (B.1), as

$$u(\mathbf{r}_i, \omega) = u_{\text{amb}}(\mathbf{r}_i, \omega) + \sum_{j=1}^{n} f_j u_j(\mathbf{f}, \omega) o_j(\mathbf{r}_i, \omega). \tag{B.8}$$

Define the matrices $\mathbf{G_R}$ and $\mathbf{G_D}$ corresponding to the sets of receiver points (denoted by $\mathcal{R}$) and object domain points (denoted by $\mathcal{D}$) respectively, as follows:

$$G_R(i, j) = o_j(\mathbf{r}_i, \omega) \qquad \text{for} \quad x_i \in \mathcal{R}$$
$$G_D(i, j) = o_j(\mathbf{r}_i, \omega) \qquad \text{for} \quad x_i \in \mathcal{D},$$

where $o_j(\mathbf{r}, \omega)$ has been defined in (B.7), and the ω dependence in the matrices on the left-hand side have been suppressed for ease of notation.

The Jacobian matrix $\mathbf{J}(\mathbf{f})$ is obtained as

$$\mathbf{J} = [\mathbf{J_{q,s}}] \tag{B.9}$$

where $[\mathbf{J_{q,s}}]$ is the stacked version of the matrices $\mathbf{J_{q,n}}$ for each source frequency ω_q, and source position s, $\mathbf{J_{q,s}}$ being given by [28]

$$\mathbf{J}_{q,s} = -\mathbf{G_R}(\mathbf{I} - \Lambda\mathbf{G_D})^{-1}\mathrm{diag}\left(\mathbf{u}^{\mathrm{int}}_{q,s}\right) \tag{B.10}$$

Using the following relation [22],

$$(\mathbf{I} - \Lambda\mathbf{G_D})^{-1} = \mathbf{I} + \Lambda(\mathbf{I} - \mathbf{G_D}\Lambda)^{-1}\mathbf{G_D} \tag{B.11}$$

we obtain a column of the Jacobian matrix as

$$\frac{\partial\vartheta}{\partial f_i} = -(G_R(:, i) + \mathbf{G_R}\Lambda\mathbf{C}^{-1}G_D(:, i))u_i(\mathbf{f}) \tag{B.12}$$

where $(:, i)$ in the argument of a matrix denotes the ith column of the matrix (in Matlab notation). Hence a second-derivative column-vector can be written as

$$\begin{aligned}\frac{\partial^2\vartheta}{\partial f_i\partial f_j} = &-(G_R(:, i) + \mathbf{G_R}\Lambda\mathbf{C}^{-1}G_D(:, i))\frac{\partial u_i(\mathbf{f})}{\partial f_j}\\ &-\left(\mathbf{G^j_R}\mathbf{C}^{-1} + \mathbf{G_R}\Lambda\left(\mathbf{C}^{-1}\mathbf{G^j_D}\mathbf{C}^{-1}\right)\right)G_D(:, i)u_i(\mathbf{f}),\end{aligned} \tag{B.13}$$

where $\mathbf{G^j_R}$ (resp. $\mathbf{G^j_D}$) is the matrix obtained by the zeroing out all columns of $\mathbf{G_R}$ (resp. $\mathbf{G_D}$) except the j th column.

References

[1] Miller E L, Kilmer M and Rappaport C 2000 A new shape based object localization and characterization from scattered field data *IEEE Trans. Geosci. Remote Sens.* **38** 1682–96

[2] Chung E T, Chan T F and Tai X C 2005 Electrical impedance tomography using level set representation and total variation regularization *J. Comput. Phys.* **205** 357–72

[3] Dorn O and Lesselier D 2006 Level set methods for inverse scattering *Inverse Problems* **22** R67–131

[4] Zacharopoulos A D, Arridge S R, Dorn O, Kolehmainen V and Sikora J 2006 Three-dimensional reconstruction of shape and piecewise constant region values for optical tomography using spherical harmonic parametrization and a boundary element method *Inverse Problems* **22** 1509–32

[5] Arridge S R, Dorn O, Kaipio J P, Kolhemainen V, Schweiger M, Tarvainen T, Vauhkonen M and Zacharopoulos A D 2006 Reconstruction of subdomain boundaries of piecewise constant coefficients of the radiative transfer equation from optical tomography data *Inverse Problems* **22** 2175–96

[6] Firoozabadi R, Miller E L, Rappaport C M and Morgenthaler A W 2007 Subsurface sensing of buried objects under a randomly rough surface using scattered electromagnetic field data *IEEE Trans. Geosci. Remote Sens.* **45** 104–17

[7] Babaeizadeh S and Brooks D H 2007 Electrical impedance tomography for piecewise constant domains using boundary element shape-based inverse solutions *IEEE Trans. Image Process.* **26** 637–47

[8] Naik N, Eriksson J, Groen P de and Sahli H 2008 A nonlinear iterative reconstruction and analysis approach to shape-based approximate electromagnetic tomography *IEEE Trans. Geosci. Remote Sens.* **46** 1558–74

[9] Wang S Y, Lim K M, Khoo B C and Wang M Y 2007 An extended level set method for shape and topology optimization *J. Comput. Phys.* **221** 395–421

[10] Santosa F 1996 A level set approach for inverse problems involving obstacles *ESAIM: Control Optim. Calc. Var.* **1** 17–33

[11] Cheney E W and Light W A 2000 *An Introduction to Approximation Theory* (Pacific Grove, CA: Brooks/Cole)

[12] Carr J C *et al* 2001 Reconstruction and representation of 3D objects with radial basis functions *Proc. Computer Graphics SiggRAPH* pp 119–26

[13] Duchon J 1977 Splines minimizing rotation invariant semi-norms in Sobolev spaces *Constructive Theory of Functions of Several Variables (Lecture Notes in Mathematics* vol 571*)* ed W Schempp and K Zeller (Berlin: Springer) pp 85–100

[14] Iske A 1995 Reconstruction of functions from generalized Hermite–Birkhoff data *Approximation Theory VIII, vol 1, Approximation and Interpolation* ed C K Chui and L L Schumaker (Singapore: World Scientific) pp 257–64

[15] Beatson R K and Langton M K 2006 Integral interpolation *Algorithms for Approximation* ed A Iske and J Levesley (Heidelberg: Springer) pp 199–218

[16] Gryazin Y A, M. V. Klibanov and T. R. Lucas 2003 Two novel numerical methods for an inverse problem for the 2D Helmholtz equation *J. Comput. Phys.* **184** 122–48

[17] Chan T F and Vese L 2001 Active contours without edges *IEEE Trans. Image Process.* **10** 266–77

[18] Rao S M and Gothard G K 1999 Integral equations *Wiley Encyclopedia of Electrical and Electronics Engineering* ed J Webster pp 351–61

[19] Naik N and Sahli H 2003 The forward problem for two-dimensional Helmholtz equation modelled GPR tomography based upon the method of moments, ETRO-IRIS Technical Report TR-089, Vrije Universiteit Brussel

[20] Kress R 1999 *Linear Integral Equations* (New York: Springer)

[21] Presley A 2001 *Elementary Differential Geometry* (Berlin: Springer)

[22] Remis R F and van den Berg P M 2000 On the equivalence of the Newton-Kantorovich and distorted Born methods *Inverse Problems* **16** L1–4

[23] Eriksson J 1996 Optimization and regularization of nonlinear least squares problems *PhD Thesis* Department of Computing Science, Umeå University, Sweden

[24] Naik N, Eriksson J and Sahli H 2004 An analysis of a Tikhonov regularized Gauss-Newton reconstruction approach to GPR tomography *Proc. 10th Int Conf. Ground Penetrating Radar, Delft, The Netherlands* 21–24 June 2004, pp 67–70

[25] Chan T F and Vese L A 2000 *Image segmentation using level sets and the Mumford-Shah model* UCLA CAM Report 00-14

[26] Blake A and Isard M 1998 *Active Contours* (London: Springer)

[27] Cheney M and Isaacson D 1995 Inverse problems for a perturbed dissipative half-space *Inverse Problems* **11** 865–8

[28] Joachimowitz N, Pichot C and Hugonin P 1991 Inverse scattering: An iterative numerical method for electromagnetic scattering *IEEE Trans. Antennas Propag.* **AP-39** 1742–52